Supporting Information

Engineering *d–p* orbital hybridization of single-atom Fe sites via axial B-mediation for enhanced oxygen reduction

Xiaoqin Xu[a], Tianmi Tang[a], Xue Bai[a], Tao Gan*[b], Jingqi Guan*[a]

[a] Institute of Physical Chemistry, College of Chemistry, Jilin University, Changchun 130021, China. *E-mail: guanjq@jlu.edu.cn (J. Guan).

[b] Shanghai Synchrotron Radiation Facility, Shanghai Advanced Research Institute, Chinese Academy of Sciences, Shanghai. *E-mail: gant@sari.ac.cn (T. Gan).

1. Material characterizations

XRD measurements (XRD-6100) and Raman (LabRAM HR Evolution) were conducted to examine the structural properties of the catalysts. TEM and HRTEM images were acquired on a JEM-2100 microscope. AC-HAADF-STEM images were recorded using a Spectra 300 microscope. SEM images were conducted using an S-4800 microscope. X-ray absorption fine structure (XAFS) spectra were acquired at the BL11B beamline of the Shanghai Synchrotron Radiation Facility (SSRF). Elemental composition and chemical states were determined via XPS on a Thermo ESCALAB 250Xi system.

2. Methods

Preparation of FePc@5-bop@ZIF-8

The synthesis procedure was as follows: First, 10 mg Iron phthalocyanine (FePc) and 60 mg 5-borondiphenic acid (5-bop) were dissolved in 20 mL ethanol under magnetic stirring for 30 min to

obtain solution A. In parallel, 1.2 g zinc nitrate and 1.2 g 2-methylimidazole were separately dissolved in 20 mL ethanol to prepare solutions B and C, respectively. Subsequently, solution C was added to solution A, followed by continued stirring for 20 min to yield solution D. Finally, solution B was introduced into solution D, and the mixture was stirred continuously for 12 h. The product was collected through three ethanol washing cycles, centrifuged, and dried under vacuum to obtain Fe Pc@5-bop@ZIF-8.

Preparation of FePc@ZIF-8

The synthesis procedure was as follows: First, 10 mg Iron phthalocyanine FePc was dissolved in 20 mL ethanol under magnetic stirring for 30 min to obtain solution A. In parallel, 1.2 g zinc nitrate and 1.2 g 2-methylimidazole were separately dissolved in 20 mL ethanol to prepare solutions B and C, respectively. Subsequently, solution C was added to solution A, followed by continued stirring for 20 min to yield solution D. Finally, solution B was introduced into solution D, and the mixture was stirred continuously for 12 h. The product was collected through three ethanol washing cycles, centrifuged, and dried under vacuum to obtain FePc @ZIF-8.

Preparation of FeN_4-B/NC and FeN_4/NC

The FePc@5-bop@ZIF-8 and FePc@ZIF-8 samples were placed in a tube furnace under a nitrogen atmosphere. The temperature was raised to 950°C and maintained for 2 hours, resulting in the production of FeN_4-B/NC and FeN_4/NC materials.

3. Electrochemical measurements

All electrochemical tests were performed on a rotating disk electrode (RDE) controller connected to an electrochemical workstation (CHI760E). A three-electrode system was used for electrochemical tests, with a saturated calomel electrode (SCE) as the reference electrode, a

platinum wire as the counter electrode, and a catalyst coated glassy carbon electrode (GCE) as the working electrode. The disc electrode was coated with the as-prepared catalyst, and the ring electrode was made of platinum. In this study, the measured SCE potential was converted to the reversible hydrogen electrode (RHE) potential based on $E_{RHE} = E_{SCE} + 0.0591\ pH + 0.241$. The method for preparing the catalyst ink was shown as follows: 2 mg of the catalyst were dispersed in a mixture of 50 μL of 5 wt.% Nafion (Aldrich) and 150 μL ethanol, and then the mixture was sonicated for 30 min to form the uniform ink. The surface of GCE (4 mm in diameter and coating area of 0.126 cm^2) was coated with 5 μL of the prepared ink to achieve a catalyst loading of 0.4 mg cm^{-2}. The area of GCE for RDE measurements is the same as that of RRDE. In this study, commercial Pt/C (20 wt.%, Hesen Electric Co., Ltd, Shanghai, China) and RuO_2 were used as the reference catalysts for ORR and OER, respectively.

3.1 ORR measurements

The ORR performance was tested in 0.1 M KOH solution. The cyclic voltammetry (CV) tests were cycled positively in the potential range from 0 to 1.2 V with a scan rate of 50 mV s^{-1}. Before each CV test, O_2 was bubbled to saturate the electrolyte. The linear sweep voltammetry (LSV) tests were performed at 1600 rpm (50 mV s^{-1}) in the O_2-saturated electrolyte.[1] The Tafel tests were carried out in an O_2-saturated electrolyte at 1600 rpm. Based on the LSV curve, the corresponding Tafel diagram could be drawn.[2] The slope was determined by the following Tafel equation:

$$\eta = a + b\log|J| \quad (1)$$

where η is the overpotential, a was the overpotential value when the current density is a unit value (1A/cm^2), b is the Tafel slope, and J was the current density.

$$\text{Slope } (d\log j/d\eta) \text{ for cathodic reaction} = (2.303RT/-\alpha_C nF) \quad (2)$$

$$\text{Slope } (d\log j/d\eta) \text{ for anodic reaction} = (2.303RT/-\alpha_A nF) \quad (3)$$

where α_C and α_A are the charge transfer coefficients for the cathodic and anodic reactions, respectively, n is the number of electrons transferred, F is the Faraday constant (96500 C), R is the ideal gas constant, T is the absolute temperature in K and η is the overpotential.

RDE measurements were conducted by varying the rotation rates (from 400 to 2500 rpm). The Koutecky-Levich (K-L) equation was used to analyze the obtained RDE data, and the transferred electron number (n) was obtained using equations 4 and 5.[3]

$$\frac{1}{j} = \frac{1}{j_L} + \frac{1}{j_K} = \frac{1}{B\omega^{1/2}} + \frac{1}{nFkC_O} \quad (4)$$

$$B = 0.62nFC_O D_O^{2/3} v^{-1/6} \quad (5)$$

where j represents the measured value of the disk current density; j_L represents the measured value of the diffusion limit current density; j_K represents the measured value of the kinetic-limiting current density; ω is the angular speed of rotating electrode; F represents the Faraday constant (F = 96485 C mol^{-1}); k is the electron-transfer rate constant; C_O is the oxygen concentration in the test solution (0.1 M KOH, C_O= 1.2 × 10^{-6} mol cm^{-3}); D_O is the oxygen diffusion coefficient in the test solution (0.1 M KOH, D_O= 1.9 × 10^{-5} cm^2 s^{-1}), and υ is the kinematic viscosity of 0.1 M KOH (υ = 0.01 cm^2 s^{-1}).

The tests for electrochemical impedance spectroscopy (EIS) and chronoamperometry (CA) were conducted at 0.8 V (1600 rpm) in an O_2-saturated 0.1 M KOH. The accelerated durability tests (ADT) were carried out to investigate the durability of the catalyst after 5000 cycles of CV tests, and LSV results were compared before and after the ADT. RRDE measurements were also carried out in O_2-saturated 0.1 M KOH electrolyte at a scan rate of 5 mV s^{-1} at 1600 rpm. The hydrogen peroxide yield (%) and electron transfer number (n) were obtained from the RRDE voltammograms using the following equations 6 and 7.

$$n = 4 \times \frac{I_d}{I_d + (I_r/N)} \quad (6)$$

$$H_2O_2\% = 200 \times \frac{I_r/N}{I_d + (I_r/N)} \quad (7)$$

Where I_d and I_r are the disk current and the ring current, respectively; N is the H_2O_2 collection efficiency of the Pt ring with the value of 0.37.

The TOF was then calculated using the formula:

$$TOF = \frac{j_K * A}{nFx_a} = \frac{j_K * A}{nF\frac{m}{M}}$$

j_K: the kinetic current densities j_K, mA cm^{-2} ,

A: the working electrode area, cm^2,

n: is the electron transfer numbers,

F: the Faraday constant, 96458 $C \cdot mol^{-1}$,

Xa: the number of active sites,

M: the mass of the active sites,

M: the relative atomic mass of the active sites.

3.2 Fabrication of home-made AZABs

The AZABs were assembled under ambient alkaline conditions (6.0 M KOH + 0.2 M zinc acetate). A mechanically polished zinc plate served as the anode, while the air electrode was constructed using a multilayered composite substrate comprising hydrophobic carbon paper, a waterproof membrane, and nickel foam (commercially sourced from Changsha Spring New Energy Technology Co., Ltd). For cathode fabrication, a homogeneous catalyst ink was formulated by

blending 5.0 mg of FeN_4-B/NC powder with 1.0 mL ethanol and 50.0 μL 1.0 wt% Nafion solution (Sigma-Aldrich), followed by uniform coating onto the composite substrate (geometric area: 1 cm^2) via a drop-casting method. The active material loading was precisely controlled at 1.0 mg cm^{-2} through gravimetric analysis. Electrochemical characterization included linear sweep voltammetry (LSV) at 10 mV s^{-1} to obtain polarization curves and galvanostatic charge-discharge cycling tests on a CT-2001A battery analyzer (LAND Electronics).

3.3 Assembly of home-made FZABs

The GPE was synthesized through a sequential procedure: Poly(vinyl alcohol) (PVA) powder (2.0 g) was dissolved in 20 mL of deionized water under continuous magnetic agitation at 90 °C for 1 h to achieve a homogeneous solution. Subsequently, a sequential addition of 18.0 M KOH and 0.2 M zinc acetate ($Zn(Ac)_2$) was achieved by introducing an aqueous solution (2 mL) into the mixture. The precursor solution was mechanically agitated for 30 min, casted into a mold and cryogenically treated at −20 °C for 2 h. The final PVA-based electrolyte membrane was obtained upon thawing under ambient conditions. For the fabrication of FZABs, a polished zinc foil served as the anode. The air cathode was prepared by coating catalyst ink onto porous composite substrates using a drop-casting method, achieving a controlled catalyst mass loading of 1.5 mg cm^{-2}. The device assembly involved sandwiching the PVA electrolyte between the zinc anode and catalyst-coated cathode, followed by encapsulation with two gas-permeable polymer membranes to ensure mechanical stability while maintaining oxygen accessibility.

4. Computational method

The computational investigations were carried out using DFT within the projector-augmented wave (PAW) formalism, utilizing the Vienna ab initio simulation package (VASP) for all simulations.[4] The treatment of exchange-correlation effects was carried out within the framework of

the Perdew-Burke-Ernzerhof (PBE) functional, which is on account of the generalized gradient approximation (GGA) approach.[5] T van der Waals interactions were accounted for through Grimme's DFT-D3 method, including a coordination number-dependent dispersion correction scheme.[6] Electronic wavefunctions were represented using a plane-wave basis set with a kinetic energy cutoff at 450 eV. Self-consistent field convergence was achieved with an energy tolerance of 10^{-4} eV during Kohn-Sham equation iterations. To eliminate periodic boundary artifacts, a 15 Å vacuum spacer was introduced in the direction normal to the basal plane. Reciprocal space sampling utilized a Monkhorst-Pack grid with 3×3×1 k-point density.[7] Structural optimization proceeded until Hellmann-Feynman forces on all atoms fell below 0.03 eV/Å. Reaction intermediate free energies (ΔG) were determined through the thermodynamic formalism:

$$\Delta G = \Delta E + \Delta E_{ZPE} - T\Delta S \quad (8)$$

Here, ΔE represents the adsorption energy obtained through DFT calculations. ΔEZPE and ΔS denote the relative differences in zero-point energy (ZPE) and entropy, respectively. These thermodynamic properties were computed under standard conditions, specifically at a pressure of ~1 bar (101325 Pa) for H_2 and a temperature of 298.15 K.

Table S1. Chemical compositions (wt.%) of FeN_4-B/NC and FeN_4/NC electrocatalysts obtained from XPS analysis

Catalyst	C	N	O	Fe	B
FeN_4-B/NC	74.82	13.07	9.78	0.55	1.79
FeN_4/NC	81.98	12.43	5.26	0.32	-

Table S2. EXAFS fitting parameters at the Fe K-edge for various samples

Sample	Shell	*CN*[a]	*R*(Å)[b]	σ² (Å²·10⁻³) [c]	ΔE_0(eV)[d]	R factor[e]
FeN_4-B/NC	Fe-N	3.90	1.96	0.008	0.04	0.005
FeN_4/NC	Fe-B	1.11	2.15	0.005	0.14	0.01
	Fe-N	4.00	1.92	0.006		
OCP	Fe-N	3.91	1.95	0.003	0.03	0.01
	Fe-B	1.12	2.06	0.004	0.08	
0.9 V	Fe-N	3.90	1.86	0.011	0.04	0.01
	Fe-B	1.11	2.12	0.002	0.02	
0.8 V	Fe-N	3.95	1.81	0.007	0.1	0.01
	Fe-B	1.2	2.19	0.001	0.04	
0.7 V	Fe-N	3.98	1.80	0.007	0.04	0.01
	Fe-B	1.13	2.20	0.007	0.02	

[a]*CN*: coordination number, [b]*R*: distance between absorber and backscatter atoms, [c]σ^2: Debye-Waller factor to account for both thermal and structural disorders, [d]ΔE_0: inner potential correction. *R* factor indicates the goodness of the fit. Fitting range: 3.0 < k (/Å) < 12.0 and 1.0 < R (Å)< 3.0.

Table S3. Comparison of ORR performance on various catalysts in 0.1 M KOH

Catalysts	**ORR halfwave potential (V vs. RHE)**	**Tafel slop ($mV\ dec^{-1}$)**	**Reference**
FeN_4-B/NC	0.915 (0.1 M KOH)	44	***This work***
Co SAs/N-C(900)	0.881 (0.1 M KOH)	75	[8]
Fe_1-N_4SO_2/NC	0.91 (0.1 M KOH)	49	[9]
Cr(acac)-NC-650	0.82 (0.1 M KOH)	39.2	[10]
ZnN_4-ZnN_4Cl-Cl	0.912 (0.1 M KOH)	69.1	[11]
La-Cl SAs/NHPC	0.91 (0.1 M KOH)	50.4	[12]
FePc-Cl-CNTs	0.91 (0.1 M KOH)	32.23	[13]
Fe_1N_4-B-C	0.87	62	[14]

	(0.1 M KOH)		
Co-N-C@HCNT	0.86	62.9	[15]
	(0.1 M KOH)		

Table S4. Comparison of rechargeable liquid Zn-air batteries performance of this work with other state-of-art electrocatalysts

Catalyst	Power density (mW cm^{-2})	Specific capacity (mAh gZn^{-1})	Durability	Reference
FeN_4-B/NC	**186**	**790.8@10 mA cm^{-2}**	**300h@10 mA cm^{-2}**	**This work**
P/Fe–N–C	269	785@20 mA cm^{-2}	192 h@10 mA cm^{-2}	16
Fe_{SA}/AC@HNC	171.5	811.8@20 mA cm^{-2}	130 h@5 mA cm^{-2}	17
FePc-Cl-CNTs	183.5	797.16@20 mA cm^{-2}	150 h@5 mA cm-2	18
ZnCoFe-N-C	137.8	931.8@50 mA cm^{-2}	90 h(@50 mA cm^{-2})	19
CoFeCu-TAC	208	806.45	125 h@10 mA cm^{-2}	20
Fe_2/Ni−N−HCMs	238.3	914.2	200 h@5 mA cm^{-2}	21
ZnCoFe-TAC/SNC	304	760@5 mA cm^{-2}	40h@5 mA cm^{-2}	22
PtFeCo/NC	187.5	791	188 h@3 mA cm^{-2}	23

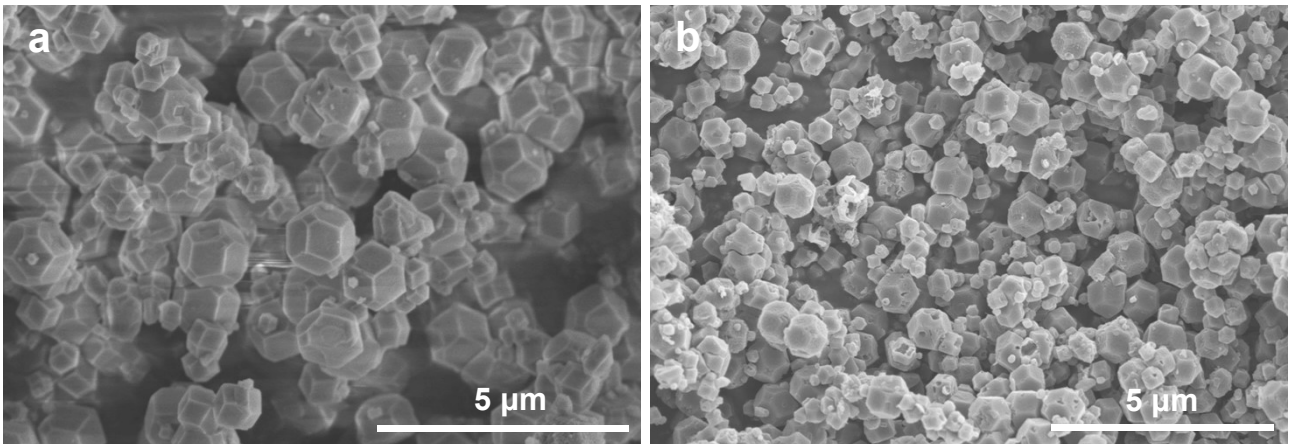

Figure S1. SEM images of (a) Fe Pc@5-bop@ZIF-8 and (b) FeN_4-B/NC.

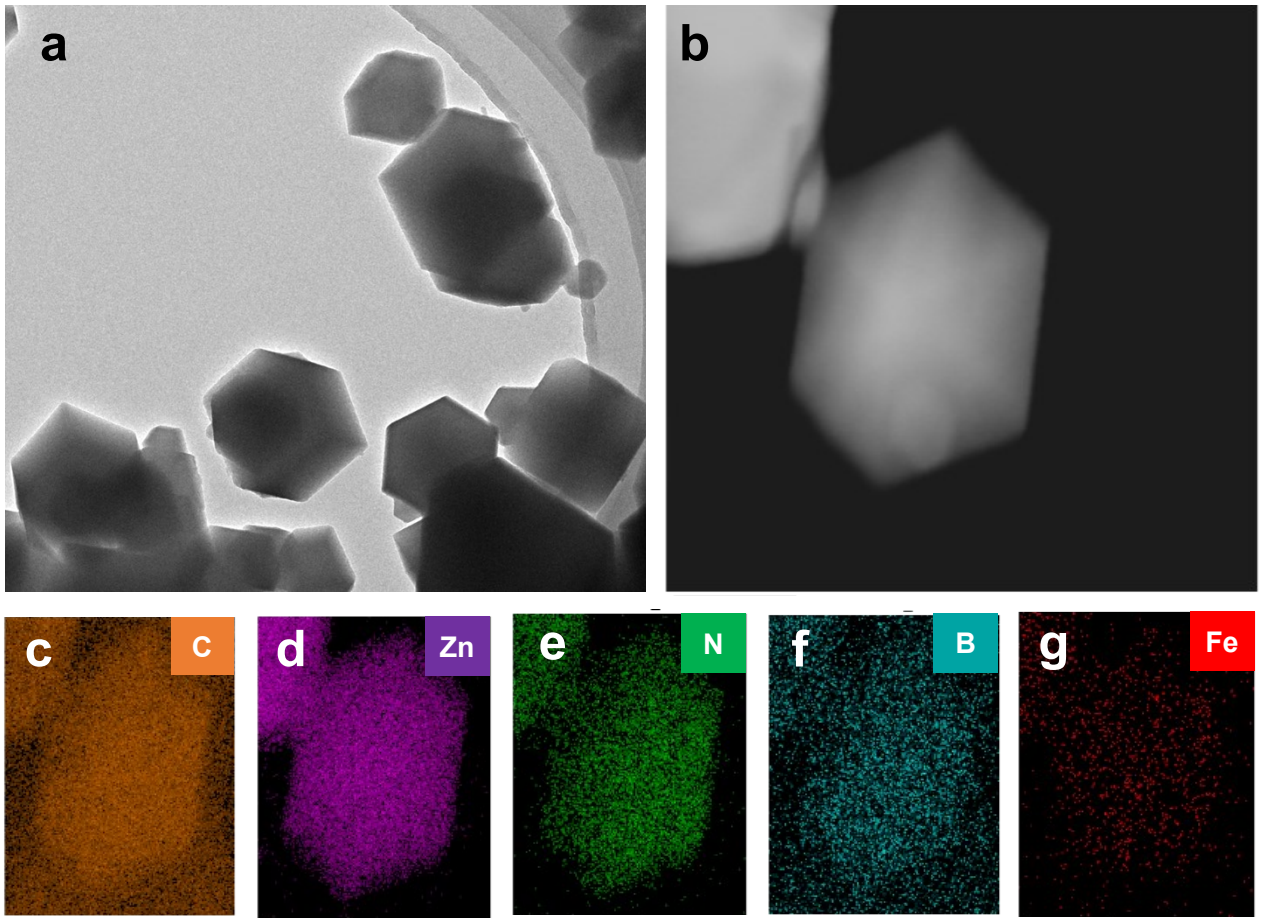

Figure S2. (a) TEM images, (b) HAADF-STEM and (c) EDS mapping of Fe Pc-5-bop@ZIF-8.

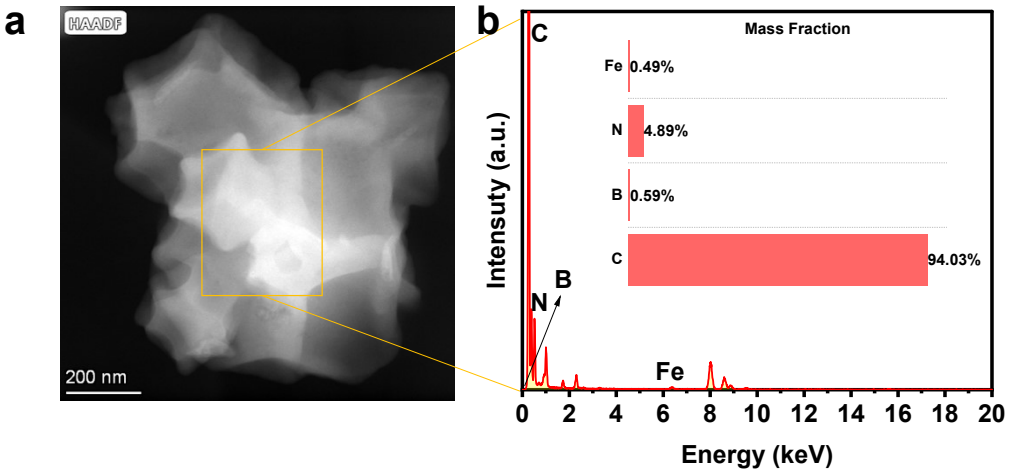

Figure S3. (a) HAADF-STEM and (b) EDS energy spectrum diagram of FeN_4-B/NC.

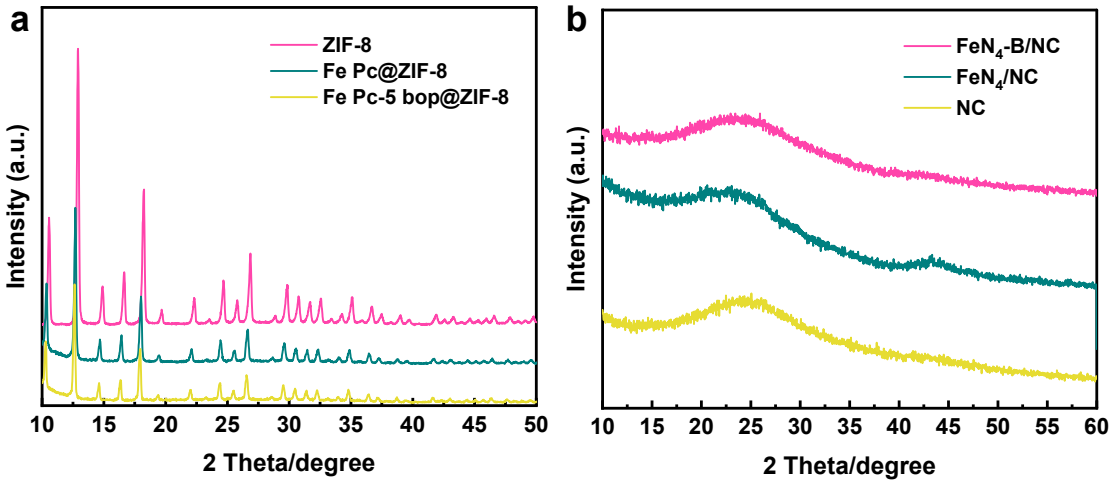

Figure S4. a) XRD patterns of ZIF-8, Fe Pc@ZIF-8 and Fe Pc@5-bop@ZIF-8. b) XRD patterns of NC, FeN_4/NC and FeN_4-B/NC.

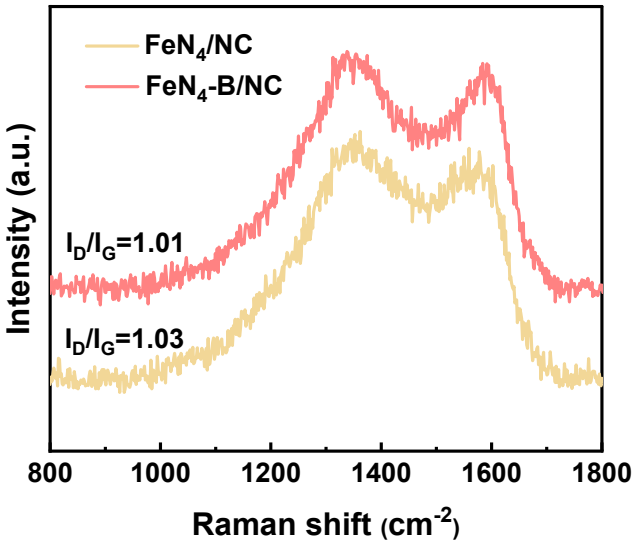

Figure S5. Raman spectra of FeN_4/NC and FeN_4-B/NC.

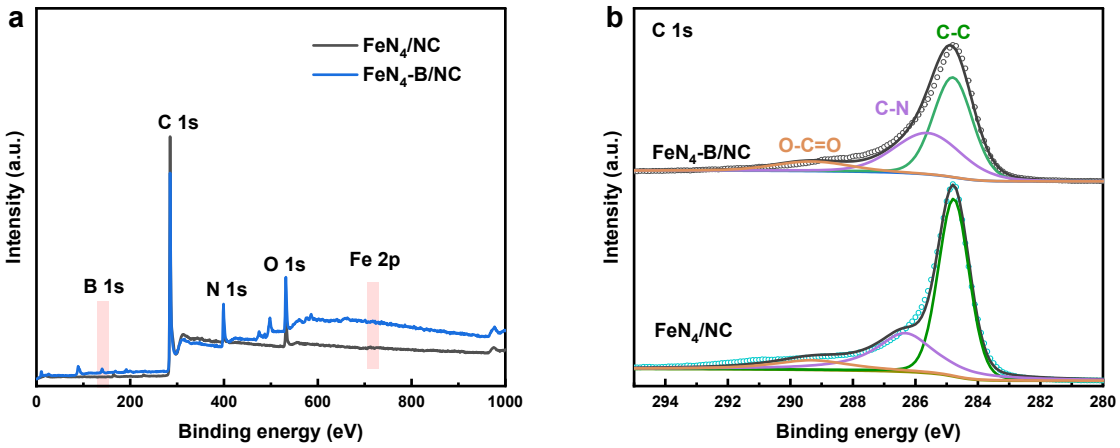

Figure S6. a) XPS survey spectra. b) High resolution XPS spectra of C 1s.

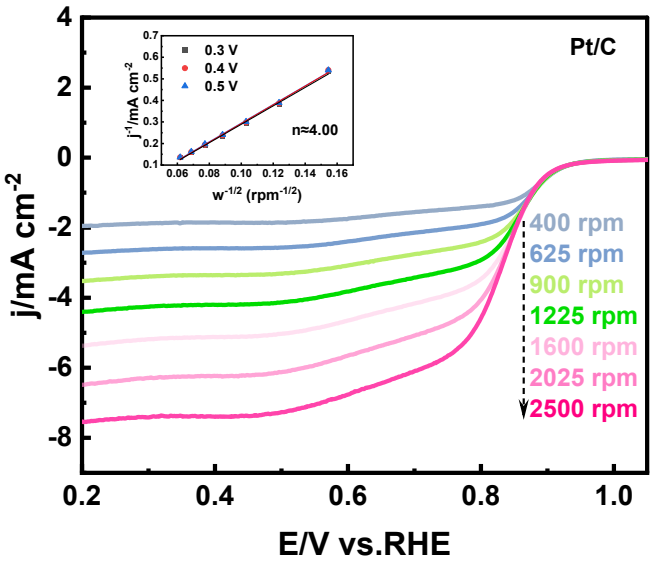

Figure S7. RDE of Pt/C.

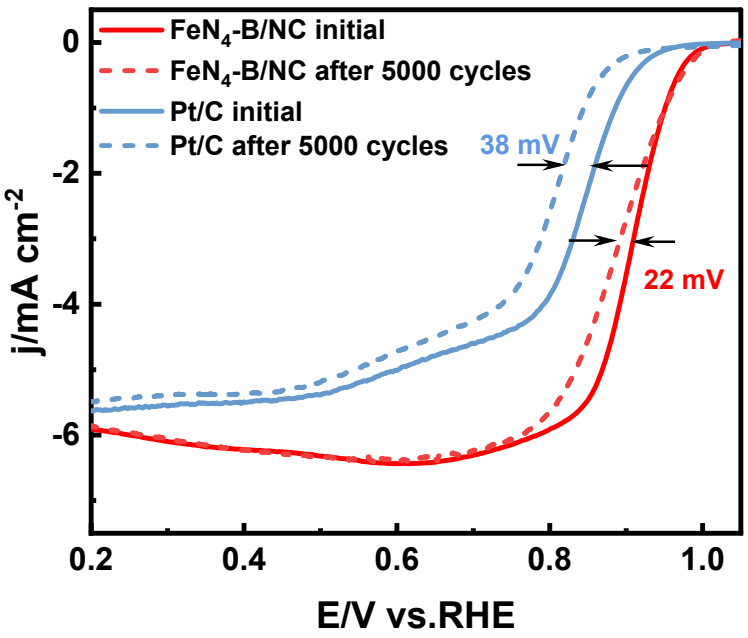

Figure S8. LSV of Pt/C and FeN_4-B/NC before and after CV testing.

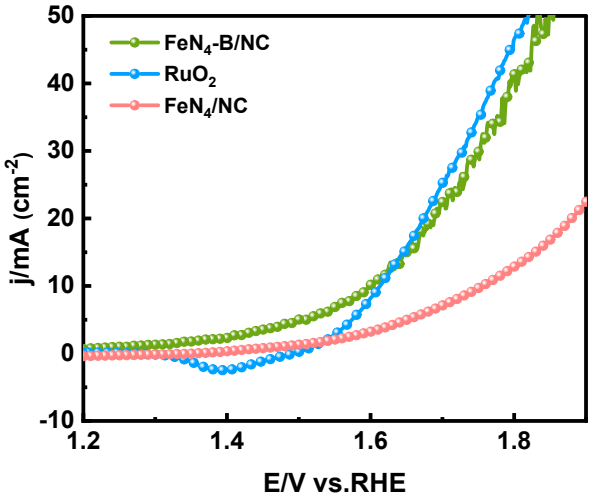

Figure S9. LSV of FeN_4-B/NC, FeN_4/NC and RuO_2 in 1 M KOH.

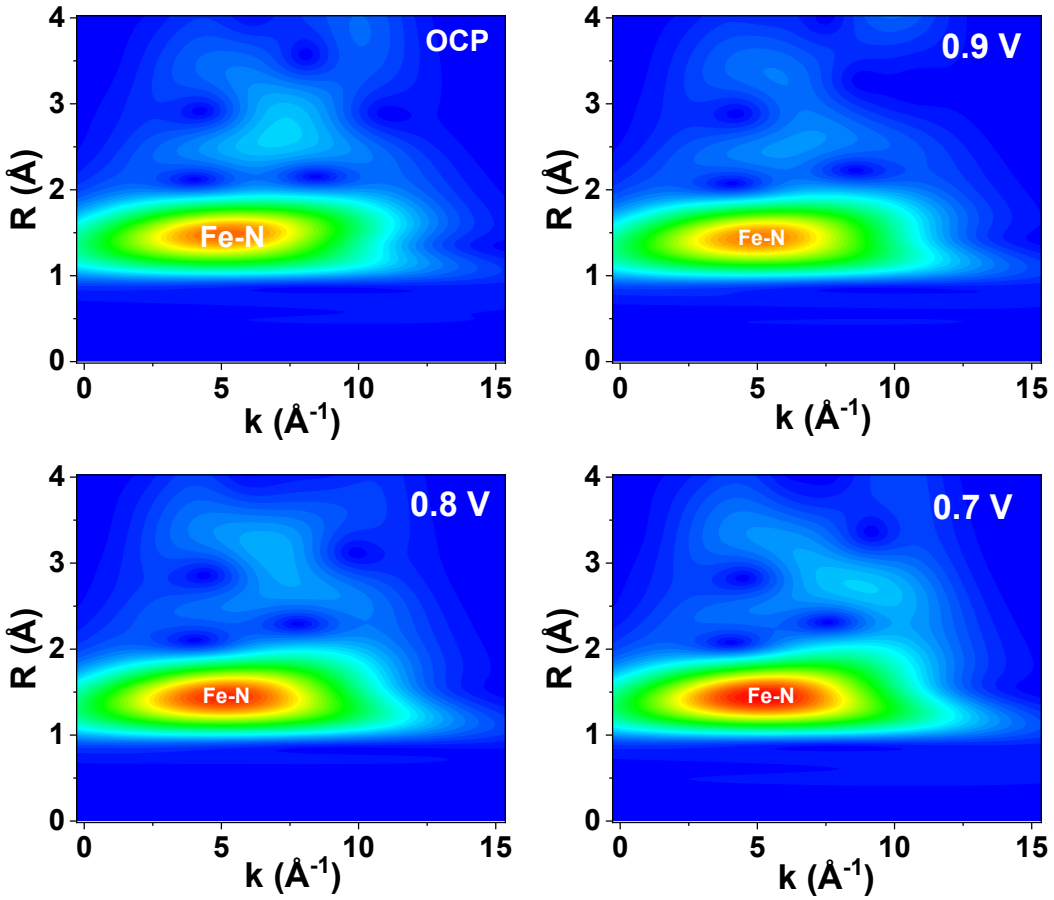

Figure S10. WT plots of FeN_4-B/NC at OCP, 0.9 V, 0.8 V and 0.7 V.

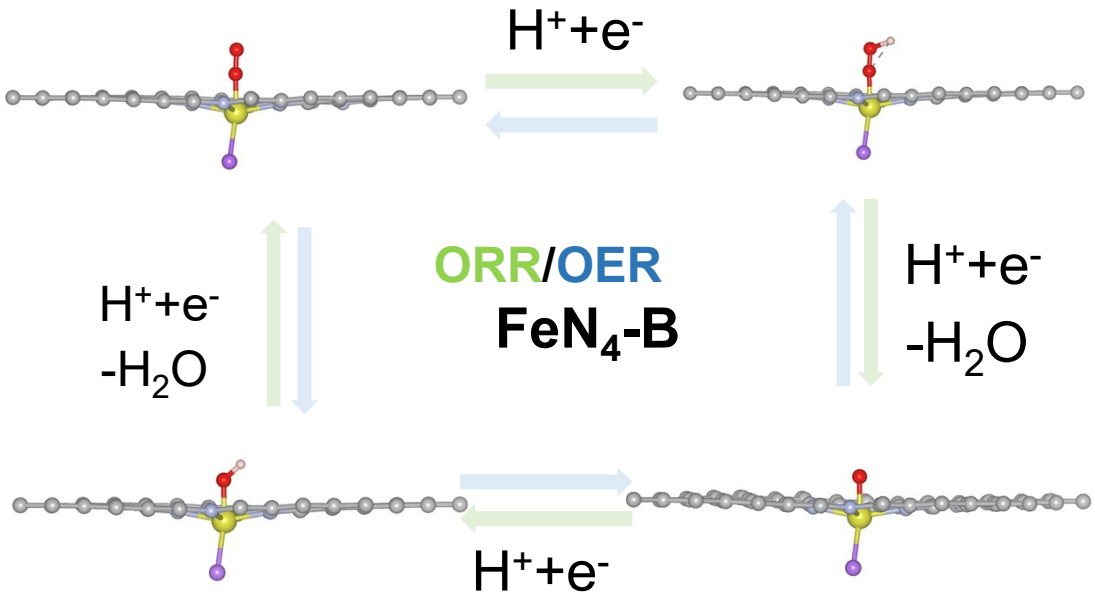

Figure S11. The ORR/OER adsorption pathway of FeN_4-B.

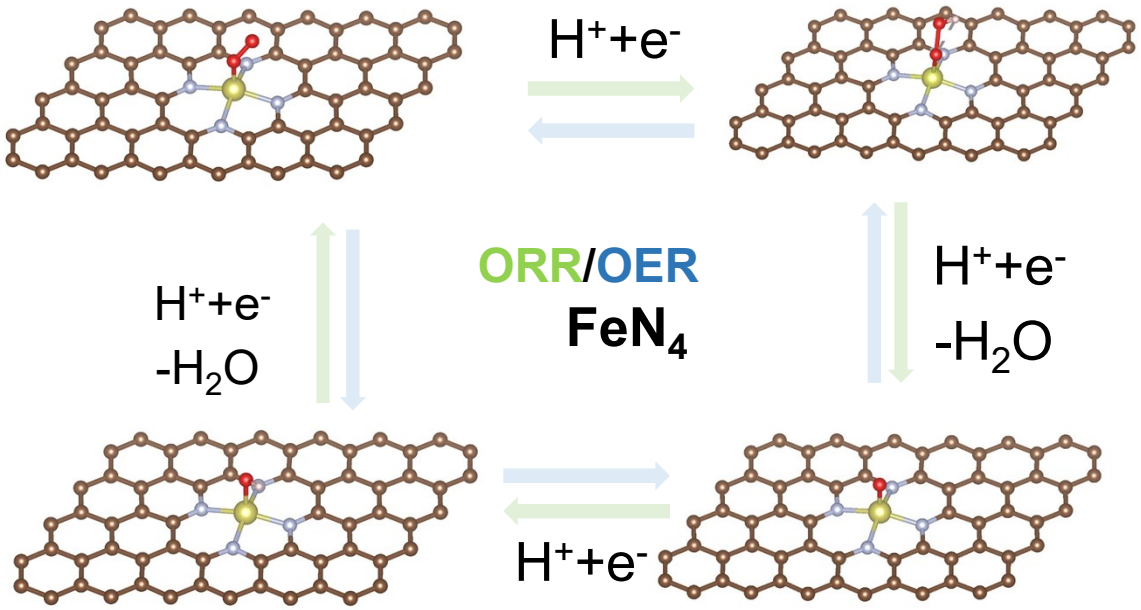

Figure S12. The ORR/OER adsorption pathway of FeN_4.

References

1. B. Ravel and M. Newville, *Athena, artemis, hephaestus: Data analysis for x-ray absorption spectroscopy using ifeffit*, *J Synchrotron Radiat*, 2005, **12**, 537-541.
2. X. Li, S. You, J. Du, Y. Dai, H. Chen, Z. Cai, N. Ren and J. Zou, *Zif-67-derived co3o4@carbon protected by oxygen-buffering ceo2 as an efficient catalyst for boosting oxygen reduction/evolution reactions*, *J. Mater. Chem. A*, 2019, **7**, 25853-25864.
3. J. Du, S. You, X. Li, B. Tang, B. Jiang, Y. Yu, Z. Cai, N. Ren and J. Zou, *In situ crystallization of active niooh/coooh heterostructures with hydroxide ion adsorption sites on velutipes-like cose/nise nanorods as catalysts for oxygen evolution and cocatalysts for methanol oxidation*, *ACS Appl. Mater. Interfaces*, 2020, **12**, 686-697.
4. G. Kresse and D. Joubert, *From ultrasoft pseudopotentials to the projector augmented-wave method*, *Physical Review B*, 1999, **59**, 1758-1775.
5. J. P. Perdew, K. Burke and M. Ernzerhof, *Generalized gradient approximation made simple*, *Phys Rev Lett*, 1996, **77**, 3865-3868.
6. S. Grimme, J. Antony, S. Ehrlich and H. Krieg, *A consistent and accurate ab initio parametrization of density functional dispersion correction (dft-d) for the 94 elements h-pu*, *J Chem Phys*, 2010, **132**, 154104.
7. H. J. Monkhorst and J. D. Pack, *Special points for brillouin-zone integrations*, *Physical Review B*, 1976, **13**, 5188-5192.

8. P. Yin, T. Yao, Y. Wu, L. Zheng, Y. Lin, W. Liu, H. Ju, J. Zhu, X. Hong, Z. Deng, G. Zhou, S. Wei and Y. Li, *Single cobalt atoms with precise n-coordination as superior oxygen reduction reaction catalysts*, *Angew. Chem. Int. Ed.*, 2016, **55**, 10800-10805.

9. Q. Qu, Y. Mao, S. Ji, J. Liao, J. Dong, L. Wang, Q. Wang, X. Liang, Z. Zhang, J. Yang, H. Li, Y. Zhou, Z. Wang, G. I. N. Waterhouse, D. Wang and Y. Li, *Engineering the lewis acidity of fe single-atom sites via atomic-level tuning of spatial coordination configuration for enhanced oxygen reduction*, *Journal of the American Chemical Society*, 2025, **147**, 6914-6924.

10. J. Luo, Y. Zhang, Z. Lu, C. Liu, Y. Xu, H. Chen, Q. Wang, D. Wu, D. Dang, Y. Deng, P. Rao, P. Deng, J. Li, Z. Miao and X. Tian, *Oxygen-coordinated cr single-atom catalyst for oxygen reduction reaction in proton exchange membrane fuel cells*, *Angew. Chem. Int. Ed.*, 2025, **64**, e202500500.

11. X. Sun, X. Li, H. Huang, W. Lu, X. Xu, X. Cui, L. Li, X. Zou, W. Zheng and X. Zhao, *Fine engineering of d-orbital vacancies of znn4 via high-shell metal and nonmetal single-atoms for efficient and poisoning-resistant orr*, *Nano Lett.*, 2024, **24**, 14602-14609.

12. L. Yin, M. Sun, S. Zhang, Y. Huang, B. Huang and Y. Du, *Chlorine axial coordination activated lanthanum single atoms for efficient oxygen electroreduction with maximum utilization*, *Adv. Mater.*, 2025, **37**, 2416387.

13. M. Liu, Y. Liu, X. Zhang, L. Li, X. Xue, M. Humayun, H. Yang, L. Sun, M. Bououdina, J. Zeng, D. Wang, R. Snyders, D. Wang, X. Wang and C. Wang, *Altering the symmetry of*

fe–n–c by axial cl-mediation for high-performance zinc–air batteries, *Angew. Chem. Int. Ed.*, 2025, **n/a**, e202504923.

14. Y. Yang, G. Wang, S. Zhang, C. Jiao, X. Wu, C. Pan, J. Mao and Y. Liu, *Boron in the second coordination sphere of fe single atom boosts the oxygen reduction reaction*, *ACS Appl. Mater. Interfaces*, 2024, **16**, 16224-16231.

15. J. Zhang, Y. Mou, W. Suo, S. Yang, J. Shen, H. Xu, Z. Zeng, R. Zhang, Z. Liang, Y. Wang, H. Zheng, J. Cao and R. Cao, *Single-atomic co-n-c sites anchored on helical carbonaceous nanotubes for the oxygen reduction reaction*, *Adv. Funct. Mater.*, 2025, **35**, 2417621.

16. Y. Zhou, R. Lu, X. Tao, Z. Qiu, G. Chen, J. Yang, Y. Zhao, X. Feng and K. Müllen, *Boosting oxygen electrocatalytic activity of fe–n–c catalysts by phosphorus incorporation*, *Journal of the American Chemical Society*, 2023, **145**, 3647-3655.

17. H. Zhang, H.-C. Chen, S. Feizpoor, L. Li, X. Zhang, X. Xu, Z. Zhuang, Z. Li, W. Hu, R. Snyders, D. Wang and C. Wang, *Tailoring oxygen reduction reaction kinetics of fe−n−c catalyst via spin manipulation for efficient zinc–air batteries*, *Adv. Mater.*, 2024, **36**, 2400523.

18. M. Liu, Y. Liu, X. Zhang, L. Li, X. Xue, M. Humayun, H. Yang, L. Sun, M. Bououdina, J. Zeng, D. Wang, R. Snyders, D. Wang, X. Wang and C. Wang, *Altering the symmetry of fe–n–c by axial cl-mediation for high-performance zinc–air batteries*, *Angew. Chem. Int. Ed.*, 2025, **64**, e202504923.

19. X. Lin, Q. Li, Y. Hu, Z. Jin, K. M. Reddy, K. Li, X. Lin, L. Ci and H.-J. Qiu, *Revealing atomic configuration and synergistic interaction of single-atom-based zn-co-fe trimetallic sites for enhancing oxygen reduction and evolution reactions*, *Small*, 2023, **19**, 2300612.

20. J. Zhong, Z. Liang, N. Liu, Y. Xiang, B. Yan, F. Zhu, X. Xie, X. Gui, L. Gan, H. B. Yang, D. Yu, Z. Zeng and G. Yang, *Engineering symmetry-breaking centers and d-orbital modulation in triatomic catalysts for zinc-air batteries*, *ACS Nano*, 2024, **18**, 5258-5269.

21. G. Yang, M. Fan, Q. Liang, X. He, W. Zhang and T. Asefa, *Atomically dispersed fe2 and ni sites for efficient and durable oxygen electrocatalysis*, *Angew. Chem. Int. Ed.*, 2024, **64**, e202421168.

22. C. Chen, J. Chai, M. Sun, T. Guo, J. Lin, Y. Zhou, Z. Sun, F. Zhang, L. Zhang, W. Chen and Y. Li, *An asymmetrically coordinated zncofe hetero-trimetallic atom catalyst enhances the electrocatalytic oxygen reaction*, *Energy Environ. Sci.*, 2024, **17**, 2298-2308.

23. R. Li, C. Gu, P. Rao, P. Deng, D. Wu, J. Luo, J. Li, Z. Miao, C.-w. Zheng, C. Shen and X. Tian, *Ternary single atom catalysts for effective oxygen reduction and evolution reactions*, *Chem. Eng. J.*, 2023, **468**, 143641.